GBT-based semi-analytical solutions for the elastic/plastic stability analysis of stainless steel thin-walled columns exposed to fire

R. Gonçalves, R. Marçalo Neves
CERIS and Departamento de Engenharia Civil, Universidade Nova de Lisboa, Portugal

D. Camotim
CERIS, DECivil, Instituto Superior Técnico, Universidade de Lisboa, Portugal

ABSTRACT: This paper presents and illustrates the application of an efficient Generalized Beam Theory (GBT) semi-analytical solution procedure to determine elastic and plastic bifurcation loads (linear stability analysis) of stainless steel thin-walled members subjected to uniform compression and exposed to fire. Besides global (flexural or flexural-torsional) buckling, the proposed GBT formulation allows for cross-section deformation and therefore makes it possible to capture local and distortional buckling. The temperature effect is taken into account using the material law for stainless steel specified in Eurocode 3 part 1-4 (CEN 2006) and Annex C of part 1-2 (CEN 2009). For plastic buckling, the material tangent moduli are obtained using both J_2 small-strain incremental and deformation plasticity theories. For illustrative purposes, the procedure is applied to columns with a lipped channel cross-section.

1 INTRODUCTION

Although initially more expensive than conventional carbon steel, stainless steel can be competitive because of its increased fire resistance, lower maintenance needs, higher corrosion resistance, better aesthetic appearance and lower life-cycle cost (SCI 2017). The fire behaviour of stainless steel members has been the subject of research of recent studies (Gardner & Baddoo 2006, Ng & Gardner 2007, Uppfeldt et al. 2008, Lopes et al. 2012). However, According to Eurocode 3, these members should be checked using the buckling interaction formulas for carbon steel members, which have been shown to be imprecise and even unsafe in some cases (Lopes et al. 2010). Moreover, studies concerning the behaviour of members with slender sections (Class 3 or 4 according to Eurocode 3), susceptible to local and/or distortional buckling, are still lacking.

To increase the knowledge on the behaviour of thin-walled stainless steel structures in case of fire, project "Fire design of stainless steel structural elements — StaSteFi" was launched in 2018 (see the acknowledgements for further details). This paper reports the first activities carried out in the context of this project, which aimed at developing a fast and accurate tool to calculate elastic and plastic buckling (bifurcation) loads/modes of thin-walled stainless steel columns (uniformly compressed members) exposed to fire and undergoing global/local/distortional buckling. The tool is based on a semi-analytical approach that relies on Generalized Beam Theory, a thin-walled bar theory that efficiently accounts for cross-section arbitrary in-plane and out-of-plane (warping) deformation through the consideration of so-called "cross-section deformation modes" (see, e.g., Schardt 1989, Camotim et al. 2010). The intrinsic non-linear stress-strain law of stainless steel, including temperature effects, is taken into account using appropriate tangent elastic moduli, based on both J_2 (von Mises) small-strain incremental and deformation plasticity theories. For illustrative purposes, the tool is applied to assess the elastic and plastic buckling behaviour of thin-walled lipped channel columns made with steel grade 1.403 and subjected to fire.

The notation in this paper follows that introduced previously, which relies on a simple vector/matrix form of the equations (Gonçalves et al. 2010b, Gonçalves & Camotim 2011, 2012). A derivative is indicated by subscript commas (e.g., $f_{,x} = \partial f / \partial x$), δ designates a virtual variation,

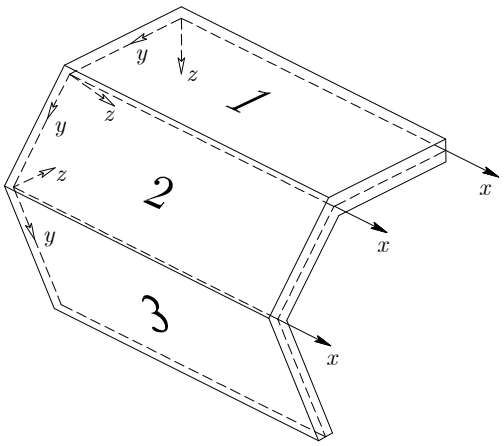

Figure 1. Arbitrary thin-walled member geometry and local coordinate systems.

Δ is an incremental variation to the buckled state, d is a generic variation and superscripts $(\cdot)^M$ and $(\cdot)^B$ are used for plate-like membrane and bending terms, respectively.

2 GBT SEMI-ANALYTICAL BIFURCATION EQUATION

2.1 *Kinematics and strain*

For an arbitrary thin-walled member, as shown in Figure 1, local axes for each wall are set, (x, y, z), defining the member axis, wall mid-line and thickness directions, respectively. According to the classic GBT kinematic description, Kirchhoff's thin plate assumption is assumed and the displacement vector $\boldsymbol{U}(x,y,z)$ for each wall is expressed as

$$\boldsymbol{U}(x,y,z) = \begin{bmatrix} U_x \\ U_y \\ U_z \end{bmatrix} = \begin{bmatrix} (\bar{\boldsymbol{u}} - z\bar{\boldsymbol{w}})^T \boldsymbol{\phi}_{,x} \\ (\bar{\boldsymbol{v}} - z\bar{\boldsymbol{w}}_{,y})^T \boldsymbol{\phi} \\ -z\bar{\boldsymbol{w}}^T \boldsymbol{\phi} \end{bmatrix}, \tag{1}$$

where $\bar{\boldsymbol{u}}(y)$, $\bar{\boldsymbol{v}}(y)$, $\bar{\boldsymbol{w}}(y)$ are column vectors containing the deformation mode displacement components along x, y and z, respectively, and $\boldsymbol{\phi}(x)$ is a column vector that contains the amplitude functions of each deformation mode along the beam length, which constitute the problem unknowns. The deformation mode displacement components are obtained from the so-called "GBT cross-section analysis", which is explained in, e.g., Gonçalves et al. 2010b, Bebiano et al. 2018, and is implemented in the `GBTUL` program, freely available at www.civil.ist.utl.pt/gbt.

The non-null small strain components for each wall are grouped in vector $\boldsymbol{\varepsilon}$, which is straightforwardly obtained from the displacements and reads

$$\boldsymbol{\varepsilon} = \begin{bmatrix} \varepsilon_{xx} \\ \varepsilon_{yy} \\ \gamma_{xy} \end{bmatrix} = \begin{bmatrix} (\bar{\boldsymbol{u}} - z\bar{\boldsymbol{w}})^T \boldsymbol{\phi}_{,xx} \\ (\bar{\boldsymbol{v}}_{,y} - z\bar{\boldsymbol{w}}_{,yy})^T \boldsymbol{\phi} \\ (\bar{\boldsymbol{u}}_{,y} + \bar{\boldsymbol{v}} - 2z\bar{\boldsymbol{w}}_{,y})^T \boldsymbol{\phi}_{,x} \end{bmatrix}, \tag{2}$$

where the terms with/without z correspond to bending/membrane deformation, respectively.

If null membrane transverse strains ($\varepsilon_{yy}^M = 0$) are assumed, which is acceptable in most beam-type problems, then $\bar{\boldsymbol{v}}_{,y} = \boldsymbol{0}$. Furthermore, if Vlasov's assumption is adopted (null membrane shear strains, $\gamma_{xy}^M = 0$), which is acceptable for open sections, then $\bar{\boldsymbol{u}}_{,y} + \bar{\boldsymbol{v}} = \boldsymbol{0}$. These two assumptions are essential to reduce the number of deformation modes (hence the problem DOFs) while ensuring that accurate results are obtained in a wide range of problems.

For the calculation of bifurcation loads, the Green-Lagrange (non-linear) longitudinal strains are required. Only the membrane component needs to be retained, which reads

$$E_{xx} \approx E_{xx}^M = \varepsilon_{xx} + \frac{1}{2}\left(\boldsymbol{\phi}_{,x}^T \left(\bar{\boldsymbol{v}}\bar{\boldsymbol{v}}^T + \bar{\boldsymbol{w}}\bar{\boldsymbol{w}}^T\right)\boldsymbol{\phi}_{,x} + \boldsymbol{\phi}_{,xx}^T \bar{\boldsymbol{u}}\bar{\boldsymbol{u}}^T \boldsymbol{\phi}_{,xx}\right). \tag{3}$$

In the latter equation, the term with $\bar{\boldsymbol{u}}\bar{\boldsymbol{u}}^T$ may be discarded without significant loss of accuracy (Gonçalves et al. 2010a). The relevant Green-Lagrange strains are therefore grouped in vector $\boldsymbol{E}^T = [E_{xx}\ \varepsilon_{yy}\ \gamma_{xy}]^T$

2.2 *Stresses and constitutive laws*

For the stresses, a plane stress state is assumed and the incremental constitutive relations between the Green-Lagrange strains and second Piola-Kirchhoff stresses are written as

$$d\boldsymbol{S} = \boldsymbol{C}_t\, d\boldsymbol{E}, \tag{4}$$

where $\boldsymbol{S}^T = [S_{xx}\ S_{yy}\ S_{xy}]$ and $\boldsymbol{C}_t$ is the tangent elastoplastic constitutive matrix for the case under consideration.

If null transverse membrane strains are assumed, the membrane and bending stresses are separated to avoid over-stiff solutions, leading to

$$d\boldsymbol{S}^M = \boldsymbol{C}_t^M\, d\boldsymbol{E}^M, \quad d\boldsymbol{S}^B = \boldsymbol{C}_t^B\, d\boldsymbol{E}^B, \tag{5}$$

where $\boldsymbol{C}_t^B = \boldsymbol{C}_t$, whereas $\boldsymbol{C}_t^M$ is calculated for $dS_{yy}^M = 0$. If Vlasov's assumption is further enforced, $\boldsymbol{C}_t^M$ is also calculated for $dS_{xy}^M = 0$, leading to a simple uniaxial law $dS_{xx}^M = E_t\, dE_{xx}^M$, where E_t is the uniaxial tangent modulus.

The small-strain J_2 (von Mises) theory is adopted, with associated flow rule and isotropic strain hardening. In the following expressions, E and G are the elastic (initial) Young and shear moduli, ν is Poisson's ratio, E_s is the secant modulus and $H' = E_t/(1 - E_t/E)$. In this case the tangent constitutive matrix for the bending terms (plane stress) is given by (Gonçalves et al. 2010a)

$$\boldsymbol{C}_t = \begin{bmatrix} C_t^{xx} & C_t^{xy} & 0 \\ & C_t^{yy} & 0 \\ \text{Sym.} & 0 & G_t, \end{bmatrix} \tag{6}$$

where the coefficients read, for the incremental (flow) theory

$$C_t^{xx} = \frac{E^2 + 4EH'}{(5-4\nu)E - (\nu^2-1)4H'}, \qquad C_t^{yy} = \frac{4E^2 + 4EH'}{(5-4\nu)E - (\nu^2-1)4H'}, \tag{7}$$

$$C_t^{xy} = \frac{2E^2 + 4\nu EH'}{(5-4\nu)E - (\nu^2-1)4H'}, \qquad G_t = G \tag{8}$$

and, for deformation theory,

$$C_t^{xx} = \frac{E^2 + (1+3e_s)EH'}{(3e_s+2-4\nu)E - (4\nu^2-3e_s-1)H'}, \tag{9}$$

$$C_t^{yy} = \frac{4E^2 + 4EH'}{(3e_s+2-4\nu)E - (4\nu^2-3e_s-1)H'}, \tag{10}$$

$$C_t^{xy} = \frac{2E^2 + 4\nu EH'}{(3e_s+2-4\nu)E - (4\nu^2-3e_s-1)H'}, \qquad G_t = G_s = \frac{E}{2\nu - 1 + 3e_s}, \tag{11}$$

where $e_s = E/E_s$. For the membrane terms the same law applies unless $d\varepsilon_{yy}^M = 0$ is assumed, in which case $dS_{yy}^M = 0$, $C_t^{xx} = E_t$ for both theories and G_t is given by G (incremental theory) or G_s (deformation theory).

For stainless steel members subjected to fire, the material law specified in Eurocode 3 part 1-4 (CEN 2006) and Annex C of part 1-2 (CEN 2009) is adopted. In the example presented in Section 3, the cross-section thickness is smaller than 6 mm. For such small values it may be assumed that the temperature is uniform over the member volume. An austenitic steel grade 1.4301 is considered, in which case one has, for a cold-rolled strip product with $t \leq 6$ mm, $E = E_a = 200$

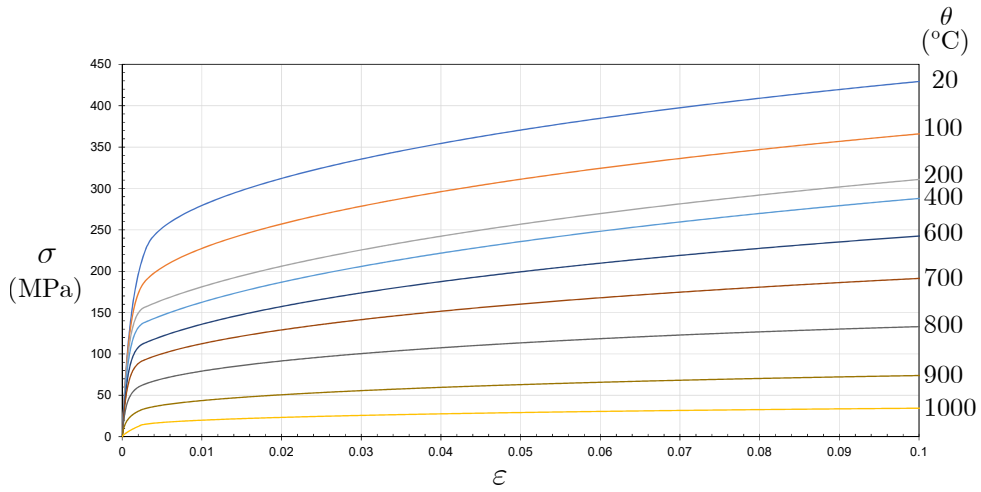

Figure 2. Uniaxial constitutive laws for the stainless steel adopted.

GPa, $\nu = 0.3$, $f_y = 230$ MPa, $f_u = 540$ MPa and the uniaxial law under fire conditions reads

$$\sigma = \frac{E_{a,\theta}\varepsilon}{1 + a\varepsilon^b}, \quad (\varepsilon \leq \varepsilon_{c,\theta}), \tag{12}$$

$$\sigma = f_{0.2p,\theta} - e + (d/c)\sqrt{c^2 - (\varepsilon_{u,\theta} - \varepsilon)^2}, \quad (\varepsilon_{c,\theta} < \varepsilon \leq \varepsilon_{u,\theta}), \tag{13}$$

where θ is the temperature, $E_{a,\theta} = E_a k_{E,\theta}$, $f_{0.2p,\theta} = f_y k_{0.2p,\theta}$, and the coefficients k_i and a-e, as well as the tangent modulus E_t, are given in Annex C of EC3 part 1-2 (CEN 2009), as a function of the temperature θ (their values and expressions are not reproduced here due to lack of space). For illustrative purposes, Figure 2 shows the uniaxial law for the stainless steel grade considered, for temperatures ranging between 20 and 1000 °C.

2.3 *Bifurcation equation*

In a linearised bifurcation analysis, the fundamental path is determined assuming geometric linearity and the bifurcation equation corresponds to an "initial stress" problem, obtained from the linearization of the virtual work equation in the direction of an incremental configuration change,

$$\Delta\left(\delta W(\boldsymbol{\phi} = \mathbf{0}, \lambda)\right) = 0, \tag{14}$$

where λ is the loading parameter. Since the displacement vector $\boldsymbol{U}$ is a linear function of $\boldsymbol{\phi}$ and $\boldsymbol{\phi}_{,x}$, only the internal part of the virtual work is non-null and the bifurcation equation reads

$$\int_V \left(\delta\boldsymbol{\varepsilon}^T \boldsymbol{C}_t \Delta\boldsymbol{\varepsilon} + \lambda \bar{S}^M_{xx}\, \Delta\delta E^M_{xx}\right) dV_0 = 0, \tag{15}$$

where V is the beam initial volume, $\bar{S}^M_{xx}$ are the membrane longitudinal normal stresses for $\lambda = 1$ and the first term must be separated into membrane and bending terms if null transverse membrane strains are assumed, as previously discussed.

In the following derivations, null transverse membrane strains/stresses are assumed. The integration of Equation 15 along the cross-section leads to a standard eigenvalue problem of the form

$$\int_L \begin{bmatrix} \delta\boldsymbol{\phi} \\ \delta\boldsymbol{\phi}_{,x} \\ \delta\boldsymbol{\phi}_{,xx} \end{bmatrix}^T \begin{bmatrix} \mathbf{B} & \mathbf{0} & \mathbf{D}_2 \\ \mathbf{0} & \mathbf{D}_1 & \mathbf{0} \\ \mathbf{D}_2^T & \mathbf{0} & \mathbf{C} \end{bmatrix} \begin{bmatrix} \Delta\boldsymbol{\phi} \\ \Delta\boldsymbol{\phi}_{,x} \\ \Delta\boldsymbol{\phi}_{,xx} \end{bmatrix} dx + \lambda \int_L \delta\boldsymbol{\phi}_{,x}^T \, \mathbf{X} \, \Delta\boldsymbol{\phi}_{,x}\, dx = 0, \tag{16}$$

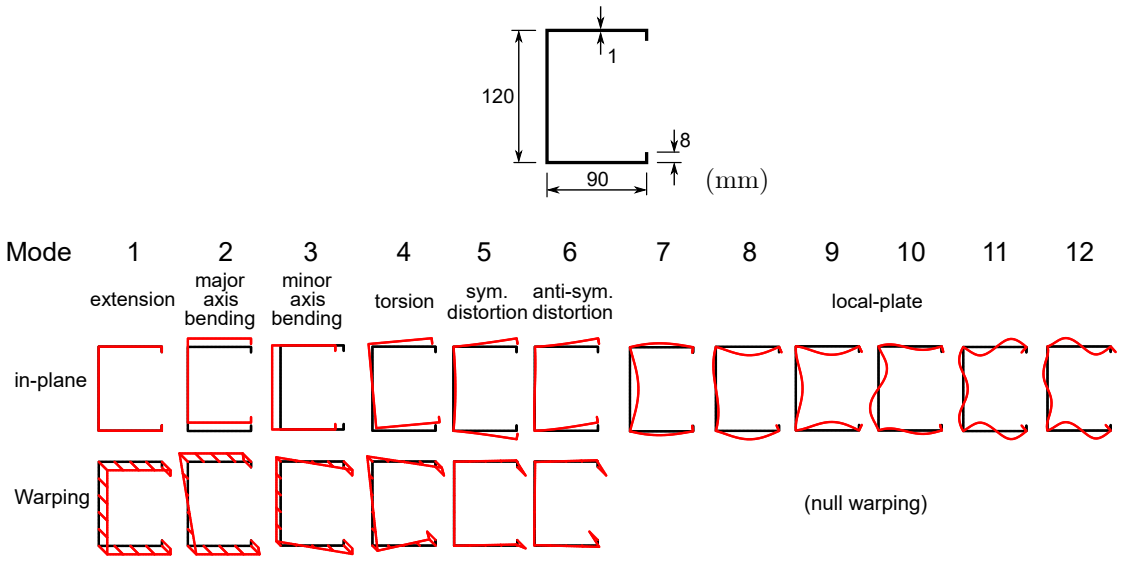

Figure 3. Lipped channel geometry (the dimensions correspond to the wall mid-line) and shapes of the first 12 GBT deformation modes.

where L is the member initial length and the GBT modal matrices are given by

$$\mathbf{B} = \int_S C_t^{yy} \tfrac{t^3}{12} \bar{\boldsymbol{w}}_{,yy} \bar{\boldsymbol{w}}_{,yy}^T \, dy, \qquad \mathbf{C} = \int_S \left(E_t t \bar{\boldsymbol{u}} \bar{\boldsymbol{u}}^T + C_t^{xx} \tfrac{t^3}{12} \bar{\boldsymbol{w}} \bar{\boldsymbol{w}}^T \right) dy, \tag{17}$$

$$\mathbf{D}_1 = \int_S G_t \left(t(\bar{\boldsymbol{u}}_y + \bar{\boldsymbol{v}})(\bar{\boldsymbol{u}}_{,y} + \bar{\boldsymbol{v}})^T + \tfrac{t^3}{3} \bar{\boldsymbol{w}}_{,y} \bar{\boldsymbol{w}}_{,y}^T \right) dy, \tag{18}$$

$$\mathbf{D}_2 = \int_S C_t^{xy} \tfrac{t^3}{12} \bar{\boldsymbol{w}}_{,yy} \bar{\boldsymbol{w}}^T \, dy, \qquad \mathbf{X} = \int_S \bar{S}_{xx}^M t(\bar{\boldsymbol{v}} \bar{\boldsymbol{v}}^T + \bar{\boldsymbol{w}} \bar{\boldsymbol{w}}^T) dy, \tag{19}$$

where S is the cross-section mid-line and t is the wall thickness. In these expressions, the membrane terms are affected by t, whereas the bending terms are multiplied by t^3.

2.4 *Semi-analytical bifurcation equation*

For simply supported members under uniform stress states, sinusoidal amplitude functions of the form $\Delta\phi_k = \bar{\phi}_k \sin(n\pi x/L)$ constitute the exact solutions, where n is the number of half-waves of the buckling mode and $\bar{\phi}_k$ is the deformation mode amplitude. Substituting the exact solution into the bifurcation Equation 16 leads to

$$\left(\frac{n\pi^2}{L^2}\mathbf{C} + \mathbf{D}_1 - \mathbf{D}_2 - \mathbf{D}_2^T + \frac{L^2}{n\pi^2}\mathbf{B} + \lambda \mathbf{X} \right) \bar{\boldsymbol{\phi}} = \mathbf{0}. \tag{20}$$

This equation is quite efficient from a computational point of view, since the number of DOFs equals the number of deformation modes included. Each bifurcation load λ (eigenvalue) is associated with a buckling mode $\bar{\boldsymbol{\phi}}$ (eigenvector) whose elements correspond to the participation of each GBT deformation mode.

Since the GBT matrices depend on λ through the tangent moduli, an iterative strategy is necessary to calculate the bifurcation loads. For the calculation of the critical load (the lowest bifurcation load), the procedure increases λ and calculates the tangent moduli at each step until $|\lambda_{cr} - \lambda| < \text{TOL}$, where λ_{cr} is the critical load parameter obtained from Equation 20 at each step. To increase the speed of the procedure, the GBT matrices are initially stored *without* the tangent moduli and are updated at each step by multiplying each one with the corresponding moduli.

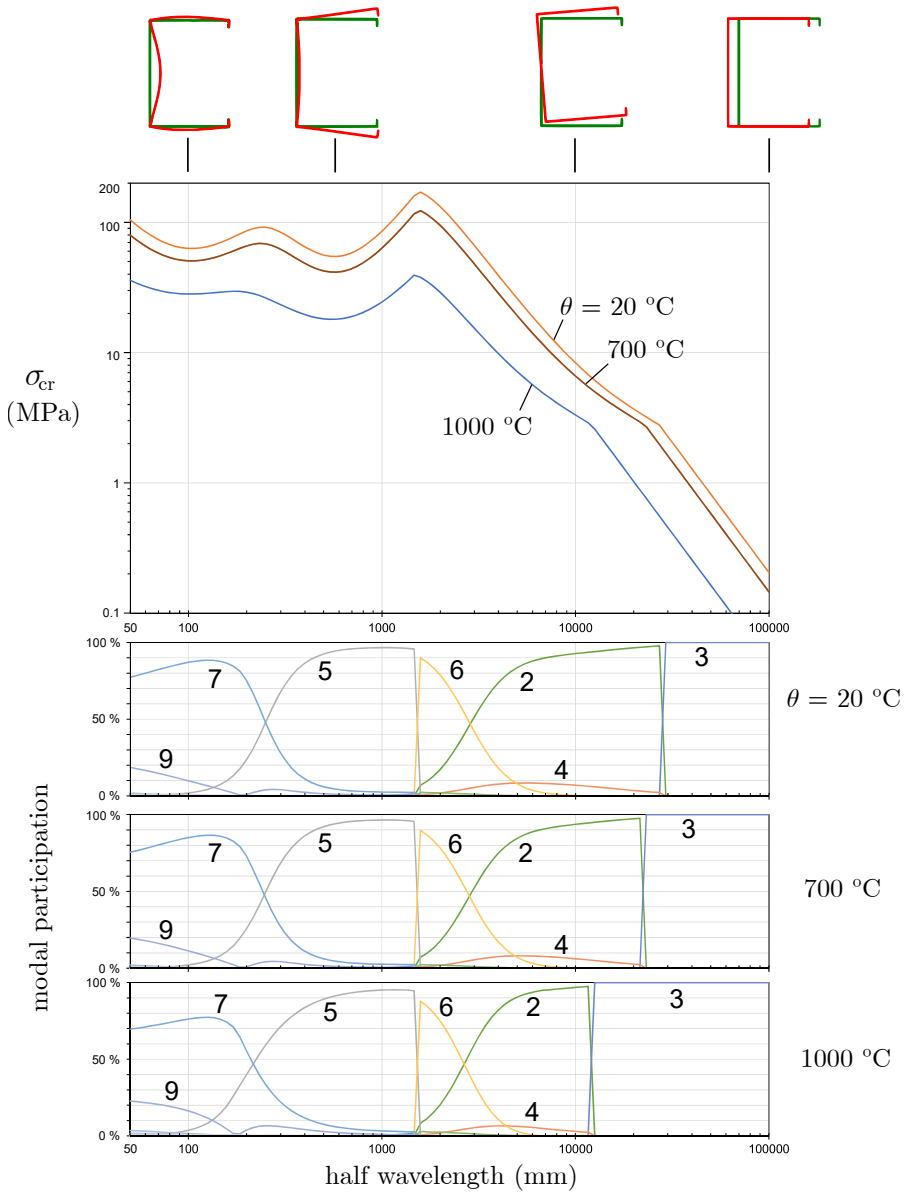

Figure 4. Lipped channel columns: signature curve, buckling modes and modal participation diagram for elastic behaviour.

3 ILLUSTRATIVE EXAMPLE

For illustrative purposes, columns with the lipped channel section shown in Figure 3 are analysed. The material properties correspond to those given in the previous section.

For the calculation of the GBT cross-section deformation modes, three/four equally spaced intermediate nodes are included in the flanges/web, respectively, leading to 48 deformation modes. However, only the so-called conventional modes (Bebiano et al. 2018) are relevant for the buckling problem under consideration and therefore are the only ones included in the analyses: 4 rigid-body modes, 2 distortional modes and 12 local-plate modes. This means that the bifurcation problem has only 18 DOFs and it is worth mentioning that all these deformation modes comply with the $\varepsilon_{yy}^{M} = 0$ and $\gamma_{xy}^{M} = 0$ assumptions. The in-plane and warping displacements of the first 12 modes are displayed in Figure 3.

First, a buckling analysis is carried out assuming a linear elastic material law with $E_t = E_{a,\theta} = E_a k_{E,\theta}$. The graphs in Figure 4 show the the critical stress as a function of the buckling mode half-wavelength (i.e. $n = 1$, the so-called "signature curve") and the temperature, as well as the GBT modal participations and the mid-span cross-section deformed configuration associated

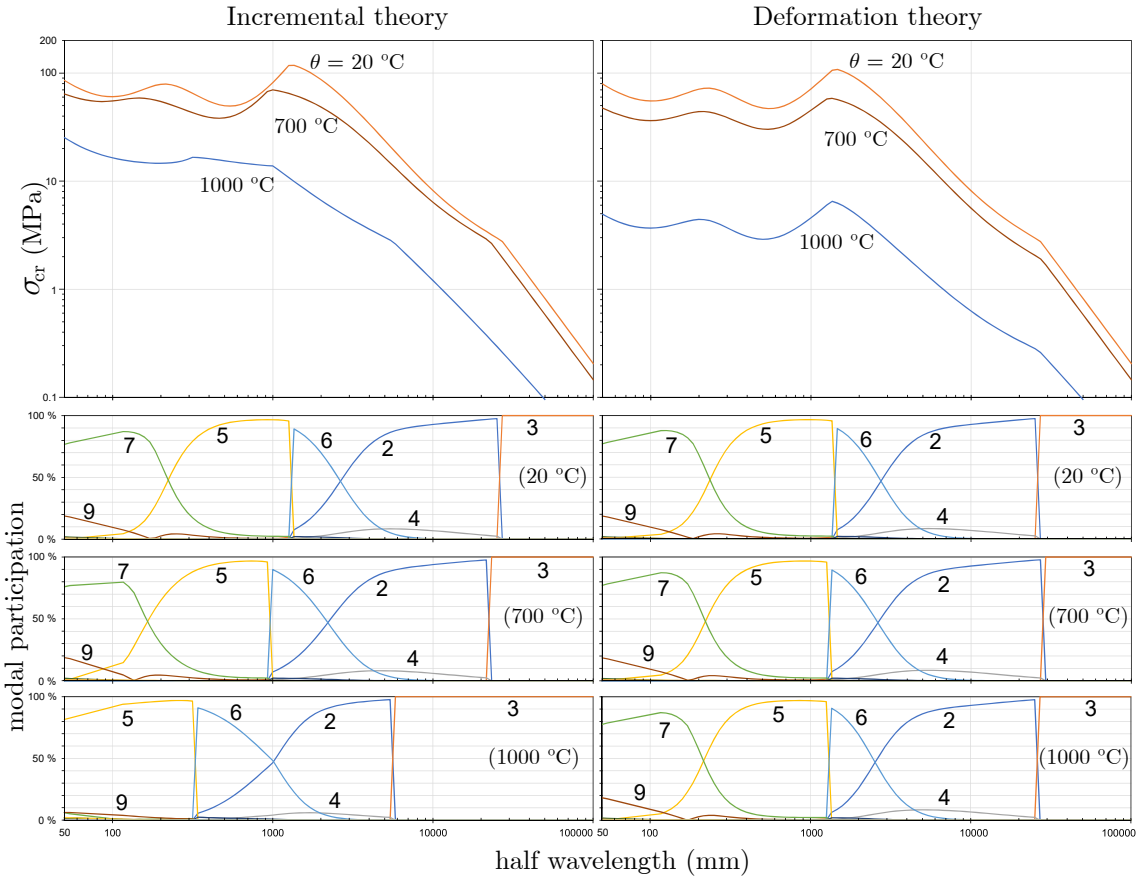

Figure 5. Lipped channel columns: signature curve and modal participation diagram for plastic behaviour.

with the elastic buckling mode for selected half-wavelengths (top of the figure). These results show a rather small variation of the critical stresses for $0 \leq \theta \leq 700$, since $k_{E,\theta} = 0.71$. However, for 1000 °C one has $k_{E,\theta} = 0.20$ and the drop in the critical stresses is significant. The modal participation graphs show that the mode transitions occur for smaller half wavelengths as the temperature increases. Nevertheless, the trend of the buckling modes is similar (from small to large half wavelengths): (i) local (7+9), (ii) symmetric distortional (5), (iii) anti-symmetric distortional-flexural-torsional (6+2+4), (iv) flexural-torsional (2+4) and finally (v) minor axis flexural.

Consider now the plastic buckling case. Figure 5 shows the results obtained for both the incremental (left) and deformation (right) theories. Although both theories yield virtually identical results for $\theta = 20$ °C, the differences increase with the temperature, with deformation theory providing the lowest critical loads, as expected (see, e.g., Gonçalves & Camotim 2004, 2007). Concerning the mode participation diagrams, in all cases the nature of the buckling mode changes with the half wavelength in a manner similar to that obtained for the elastic cases. However, it should be noted that the incremental theory predicts mode transitions for smaller half wavelengths, most remarkably for $\theta = 1000$ °C (bottom left graph), in which case the local mode (7+9) does not appear in the graph. Finally, attention is called to the fact that the "kink" appearing in the critical stress curve for the incremental theory, $\theta = 1000$ °C and $L = 1000$ mm, is not due to a change in the buckling mode shape but rather to a discontinuity of the tangent moduli for $\varepsilon_{xx} = \varepsilon_{c,\theta}$, due to the particular form of the uniaxial constitutive law adopted, given by Equations 12-13.

4 CONCLUSION

This paper reported the first activities carried out in the context of project "StaSteFi". A fast and accurate numerical tool to assess the elastic and plastic local/distortional/global bifurcation

behaviour of thin-walled stainless steel columns exposed to fire was presented. The tool is based on a GBT-based semi-analytical approach and therefore is capable of handling, efficiently and accurately, cross-section arbitrary in-plane and out-of-plane (warping) deformation with a very small computational cost. Moreover, the intrinsic non-linear stress-strain law of stainless steel, including temperature effects, can be straightforwardly taken into account using the appropriate tangent elastic moduli pertaining to J_2 small-strain incremental and deformation plasticity theories. For illustrative purposes, the elastic and plastic bifurcation behaviour of thin-walled lipped channel columns made with steel grade 1.403 and subjected to fire was assessed.

Future developments, which are already under way and will be reported in the near future, include extending the proposed GBT formulation to a finite element setting, in order to handle arbitrary loading and support conditions.

ACKNOWLEDGEMENTS

The authors gratefully acknowledge the financial support of FCT (Fundação para a Ciência e a Tecnologia, Portugal), through Project "StaSteFi — Fire design of stainless steel structural elements".

REFERENCES

Bebiano, R., Camotim, D. & Gonçalves, R. 2018. GBTUL 2.0 – a second-generation code for the GBT-based buckling and vibration analysis of thin-walled members. *Thin-Walled Structures* 124: 235-253.

Camotim, D., Basaglia, C., Bebiano, R., Gonçalves, R. & Silvestre N. 2010. Latest developments in the GBT analysis of thin-walled steel structures. In E. Batista, P. Vellasco, L. Lima (eds.), *Proceedings of International Colloquium on Stability and Ductility of Steel Structures, Rio de Janeiro, 8-10 September 2010* 33-58 (Vol. 1).

CEN 2006. *Eurocode 3 - Design of steel structures - Part 1-4: General rules - Supplementary rules for stainless steels*. Brussels, Belgium: European Committee for Standardization.

CEN 2009. *Eurocode 3 - Design of steel structures - Part 1-2: General rules - Structural fire design*. Brussels, Belgium: European Committee for Standardization.

Gardner, L. & Baddoo, N. 2006. Fire testing and design of stainless steel structures. *Journal of Constructional Steel Research* 62: 532-543.

Gonçalves, R. & Camotim, D. 2004. GBT local and global buckling analysis of aluminium and stainless steel columns. *Computers & Structures* 82(17-19): 1473-1484.

Gonçalves, R. & Camotim, D. 2007. Thin-walled member plastic bifurcation analysis using Generalised Beam Theory. *Advances in Engineering Software* 38(8-9): 637-646.

Gonçalves, R., Le Grognec, P. & Camotim, D. 2010a. GBT-based semi-analytical solutions for the plastic bifurcation of thin-walled members. *International Journal of Solids and Structures* 47(1): 34-50.

Gonçalves, R., Ritto-Corrêa, M. & Camotim, D. 2010b. A new approach to the calculation of cross-section deformation modes in the framework of Generalized Beam Theory. *Computational Mechanics* 46(5): 759-781.

Gonçalves, R. & Camotim, D. 2011. Generalised Beam Theory-based finite elements for elastoplastic thin-walled metal members. *Thin-Walled Structures* 49(10): 1237-1245.

Gonçalves, R. & Camotim, D. 2012. Geometrically non-linear Generalised Beam Theory for elastoplastic thin-walled metal members. *Thin-Walled Structures* 51: 121-129.

Lopes, N., Vila Real, P., Simões da Silva, L. & Franssen, J-M. 2010. Axially loaded stainless steel columns in case of fire. *Journal of Structural Fire Engineering* 1(1): 43-59.

Lopes, N., Vila Real, P., Simões da Silva, L. & Franssen, J-M. 2012. Numerical analysis of stainless steel beam-columns in case of fire. *Fire Safety Journal* 50: 35-50.

Ng, K. & Gardner, L. 2007. Buckling of stainless steel columns and beams in fire. *Engineering Structures* 29(5): 717-730.

Schardt, R. 1989. *Verallgemeinerte Technische Biegetheorie*. Berlin: Springer-Verlag.

SCI 2017. *Design Manual for Structural Stainless Steel, 4th Edition*, Ascot, UK: The Steel Construction Institute.

Uppfeldt, B., Outinen, T. & Veljkovic, M. 2008. A design model for stainless steel box columns in fire. *Journal of Constructional Steel Research* 64(11): 1294-1301.